Soft Matter

ARTICLE TYPE

Cite this: DOI: 00.0000/xxxxxxxxxx

Pick and release of micro-objects: a motion-free method to change the conformity of a capillary contact.†

Antonio Iazzolino,[a] Youness Tourtit,[a,b] Adam Chafaï,[b] Tristan Gilet,[a] Pierre Lambert,[b] and Loïc Tadrist,‡[a]

Received Date
Accepted Date

DOI: 00.0000/xxxxxxxxxx

We propose a new 3D-printed capillary gripper equipped with a textured surface for motion-free release. The gripper classically picks up micro-objects thanks to the capillary forces induced by a liquid bridge. Micro-objects are released by decreasing the volume of this bridge through evaporation. This latter can be either natural or speeded up by a heating source (IR laser or Joule effect). The volume reduction changes the conformity of the contact between the gripper and the object. We analyze the gripper performances and the capillary force generated, then we rationalize the release mechanism by defining the concept of contact conformity in the context of capillary forces.

1 Introduction

Many strategies to handle objects are not suitable at sub-millimeter scale. Vacuum grippers and friction grippers[1] are still predominant in pick-and-place industries. The constant miniaturization of objects makes the handling process more and more difficult, because of the associated size reduction of grippers and the difficulty to manage the positioning and handling of micro-objects without damaging them. These industries also have to comply with increasingly stringent standards on the reliability of the micro-objects they assemble.

Alternative handling mechanisms have been developed for small, fragile and soft objects. Several different physical strategies have been used to create the attractive or restoring forces necessary to handle micro-objects. Some of them allow to avoid impacts or to fit to the shape of the handled object, such as smart actuated microgel grippers[2], optical tweezers[3], grippers based on liquid-solid transition (catch-and-block strategy), Bernoulli airflow principle or acoustic levitation[1].

Capillary gripping is another promising handling mechanism that consists in taking benefits from capillary forces, dominant over gravity at the sub-millimeter scale[4]. These capillary forces are generated by a liquid meniscus that binds the object to the gripper. Their application to micro-assembly has been studied in[4] and[5]. Capillary forces result from a tension applied on the gas-liquid-solid triple line interface and the Laplace pressure jump across the interface between gas and liquid. This differential pressure is proportional to the curvature of the liquid meniscus. The current idea of using capillary forces as a gripping principle has been first developped in 1998[6] and 2002[7]. Lambert et al.[8] have demonstrated the feasibility of handling sub-millimeter balls of watch bearings. Wettability of the micro-object is preferably high to enhance the gripping ability. However Lambert[8] showed that with proper geometry of the gripper, even slightly hydrophobic components could be picked up. Higher surface tension of the handling liquid (*e.g.* water) leads to larger capillary forces. Other solvents like isopropanol, silicone oils or other organic liquids exhibit lower surface tension but a better wettability. Volatile solvents may improve gripping dynamics and also avoid residual traces of liquid after release.

Since those first works, many solutions to the control of capillary forces for gripping applications have been developed. Force control represents a major challenge for capillary handling since it establishes the ability to pick, to maintain and especially to release the handled objects. Both physical and geometrical parameters may be tuned to control capillary forces: electro-wetting[9–11] or thermal stimulation[12] modify the wettability on the substrate, while liquid feeding[13,14] or active change of gripper geometry[15] only modify the capillary bridge geometry.

Different release mechanisms have been considered in previous studies, see Table 1. Release mechanisms may be sorted in two main categories. The first involves applying an additional force to the handled part in order to break the liquid bridge. For exam-

[a] *Microfluidics Lab, Department of Aerospace and Mechanical engineering, University of Liège, Belgium*
[b] *Tranfers, Interfaces & Processes (TIPs), Université Libre de Bruxelles CP 165/67, Belgium*
† Electronic Supplementary Information (ESI) available: [details of any supplementary information available should be included here]. See DOI: 00.0000/00000000.
‡ E-mail: loic.tadrist@uliege.be

Table 1 Census of release mechanisms for capillary grippers

Ref.	Release mechanism	Release duration depending on	Minimal released weight	Size and weight of tested objects	Component possibly damaged by
[8]	Meniscus shearing	Mechanical limits of actuators *	-	S: D=0.5 mm W = $3.8\,10^{-3}$ mN	Mechanical loads *
[16]	Rotation of handled object	Mechanical limits of actuators *	-	C: 1x0.5x0.5 mm^3	Mechanical loads *
[17]	Glue on substrate	Fluid motion *	-	-	Chemical contamination *
[17]	Inertia - Vertical deceleration	Mechanical limits of actuators *	Depending on applied accelerations *	-	Mechanical loads *
[18] [19]	Inertia - Vibrations	Mechanical limits of actuators *	Depending on amplitude and frequency *	S: D=0.04-0.20 mm W=$0.35\,10^{-6}$-$43.4\,10^{-6}$ mN C: 0.5x0.5x0.28 mm^3 W=$1.63\,10^{-3}$ mN C: 1x1x0.52 mm^3 W=$12.1\,10^{-3}$ mN	Mechanical loads *
[6]	Injection of gas	Fluid motion *	-	C: 4.2x4.2x0.5 mm3 W=0.2 mN	None *
[9] [10] [20]	Electrowetting	Fluid motion *	77 mN	W=$77\,10^{-3}$-$136\,10^{-3}$ mN	Electrical current *
[15]	Stretching of the gripper	Fluid motion *	-	S: D=0.5-2.85 mm W=3–373 mN Microscrews: 0.5-2.5 mm W=28-310 mN	None *
[22] [23]	Change in conformity	Fluid motion *	0.47 mN	W=0.295-2.18 mN *	None *
[12]	Evaporation and capillary forces on substrate	Fluid motion *	No limit *	S: D=0.005-0.06 mm	None *

S: Sphere (diameter is given), C: Cuboid (lengths are given), W: Weight of object(s), *: Own estimations.

ple, meniscus shearing is studied in[8], while[16] explores a release by means of the rotation of the handled micro-part induced by the compression under uneven micrometer-sized pillars. The additional force can also be developed by inertia, e.g. in[17] where a large vertical deceleration is applied to the gripper, or in[18] and[19] where vibrations are used. The rupture of the meniscus has also been achieved by generating a higher attraction force on the substrate on which the release is expected, *e.g.* through the addition of glue[17].

The second category of solutions consists in releasing brittle micro-objects without applying additional loads on them. These solutions are based on the decrease of capillary forces. Bark[6] suggests the injection of gas in order to change the internal pressure in the meniscus. Decreasing capillary forces can also be achieved by modifying wettability: capillary forces are decreased thank to electrowetting in[10],[9] and[20]. An elastic gripper is stretched in order to modify its wettability in[15]. Based on Israelachvili's model[21],[22] and[23] have investigated the change of curvature of their grippers, also known as conformity (see Section 4.1), in order to decrease capillary forces and therefore to release objects. Heating can also lead to the decrease of capillary forces by evaporation of the meniscus. This solution is studied in[12] where this evaporation is coupled to the generation of capillary forces on the substrate.

A reliable, accurate, harmless and fast release mechanism is indeed necessary for industrial applications. An Ipulse M20 pick-and-place machine from Yamaha would for instance place one chip every 0.15 s with 4 picking heads. But contrary to inexpensive micro-objects which are mass-produced and which can be processed in fast assembly, the micro-manipulation of brittle objects must give priority to the integrity of the components.

In line with the second category of release mechanisms, this paper explores a motion-free release mechanism for capillary grippers based on a change of the conformity in the contact area. This change is allowed by surface texturing and bridge volume reduction through evaporation. The surface of the gripper is textured with small cones called barbules. They avoid the persistence of strong capillary forces when the liquid bridge volume is reduced. Indeed the persistence of capillary forces at very low liquid volume associated with dry adhesion (Van der Waals forces) may prevent release for non-textured grippers. The release ability of the gripper is thus enhanced by this surface texture.

This article first presents the set-up and methods to study this new release strategy. The experimental results are then compared to models. In particular, the concept of contact conformity is defined in the context of capillary gripping. Finally, conclusions and perspectives are discussed in section 5.

2 Materials and methods

2.1 Gripper

The gripper used for all the experiments was a cone covered with spine-like microstructures called barbules (Fig. 1b). The gripper was 3D-printed with the two-photon-initiated polymerization-based stereolithography system *Nanoscribe*, with a 200 nm resolution. The gripper material was IP-L 780 UV-curable pho-

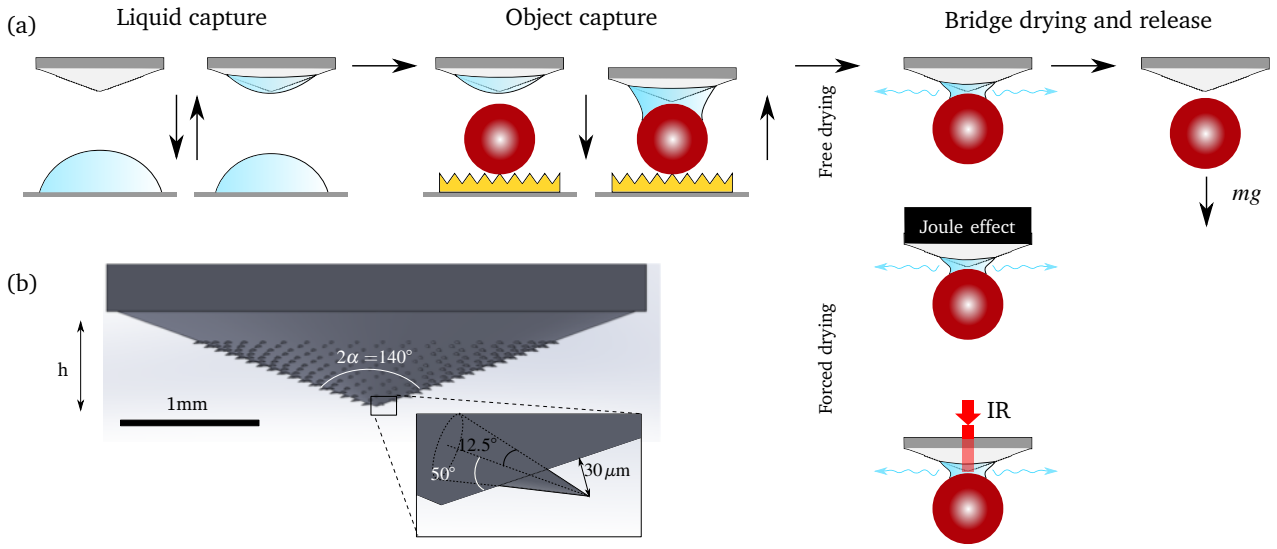

Fig. 1 (a) Schematics of the experimental procedure. First, the gripper was loaded by plunging it into a volatile liquid, here water. The gripper was then moved to create a capillary bridge between the gripper and the micro-object (here a sphere for clarity but idealized objects with a spherical cap and a cylindrical body were also considered in the experiment). Special care was taken to pick-up the micro-object from a textured surface to avoid any unwanted sticking on the surface. Finally, the object was released by drying the capillary bridge. The drying was either unforced or speeded up by heating the liquid by joule effect or with an IR-laser. (b) CAD geometry of the conical gripper. Close-up on a barbule.

toresin. The main cone had a height h of 700 μm and an aperture angle α of 140°. The barbules were also cones, of half aperture 12.5°, with a tilt angle respective to the cone surface of 50°. The distance from the surface of the cone to the head of the tip was 30 μm and the distance between two barbules was 50 μm. The barbule density was 50 barbules/mm^2.

Barbules were designed following three principles, (i) the dimension of the surface texture is less than ten times smaller than the size of the gripper/ micro-object. (ii) the barbules have a simple shape with a large aspect ratio. (iii) The barbules size is limited by the resolution of the 3D printer (400 nm). According to these criteria, we could print well-shaped conical barbules with dimensions of 30 μm, roughly 100 times the resolution of the 3D printer.

2.2 Experimental set-up

The experimental set-up is described in Fig. 1a. The gripper was mounted on a 3 degrees-of-freedom translation stage. High-precision mechanical stages were used for an accurate positioning of the gripper in the (x,y) plane. The vertical motion of the gripper was controlled with a linear actuator (*Z825B* from *Thorlabs*) with a resolution of 0.5 μm.

A droplet of approximately 10 μL of purified water was deposited on a metallic substrate. To ensure reproducibility, the substrate was cleaned with ethanol and a new droplet was deposited before each experiment. The gripper was first vertically moved (z-axis) toward the droplet to form a liquid bridge. It was then moved upwards, which stretched and broke the liquid bridge. A liquid volume of 1.9±0.4 μL was left on the gripper. Reduced volumes of liquid, ([0.7, 0.4, 0.1] μL), were obtained by drying the initial liquid bridge with an IR laser (1455 nm) at 491 mW (for [15, 20, 30] s respectively).

Idealized millimeter-sized objects, each consisting of a spherical cap on top of a vertical cylinder of radius 1 mm, were 3D-printed with a resin of density $\rho = 1.17 \times 10^3\,\mathrm{kg\,m^{-3}}$ (*VeroWhitePlusRGD 835*). Three cap radii were tested (R_1 =625 μm, R_2 =950 μm, and R_3 =1250 μm) and the mass of the objects was varied from 1 mg to 30 mg by changing the length of the cylinder. The objects were initially placed on a micro-structured planar surface. The microstructures were again conical tips, which purpose was to minimize solid-solid contact forces.

The gripper was moved downwards until a capillary bridge was formed with the object. The object then followed the gripper: it could be lifted and moved horizontally at the same time as the gripper (see video in supplementary material).

The water bridge volume was decreased, through either natural or forced evaporation. Two techniques were considered to force evaporation. The first was based on the Joule effect: an electrical current flowed in a ceramic heater plate and produced heat. The heat was transferred by conduction from the plate to the gripper then to water. The second technique involved an IR laser with a wavelength of 1455 nm. The gripper made of IP-L 780 UV-curable photoresin was indeed transparent to this wavelength. The IR light was efficiently absorbed by water with an absorption coefficient of $2.6 \times 10^3\mathrm{m}^{-1}$. The absorbed energy was turned into heat, which induced water evaporation. The maximal power of our IR-laser was 0.5 W.

The experiment was imaged from the side with a camera (*Canon EOS 5D Mark III*) and a macro lens (*Canon-MP-E 65mm f/2.8 1-5x Macro*). The resolution was 3.8 μm/pixel.

2.3 Force measurement set-up

The quasi-static capillary force was measured by the deflection of a calibrated steel cantilever. As depicted in Figure 2a, the exper-

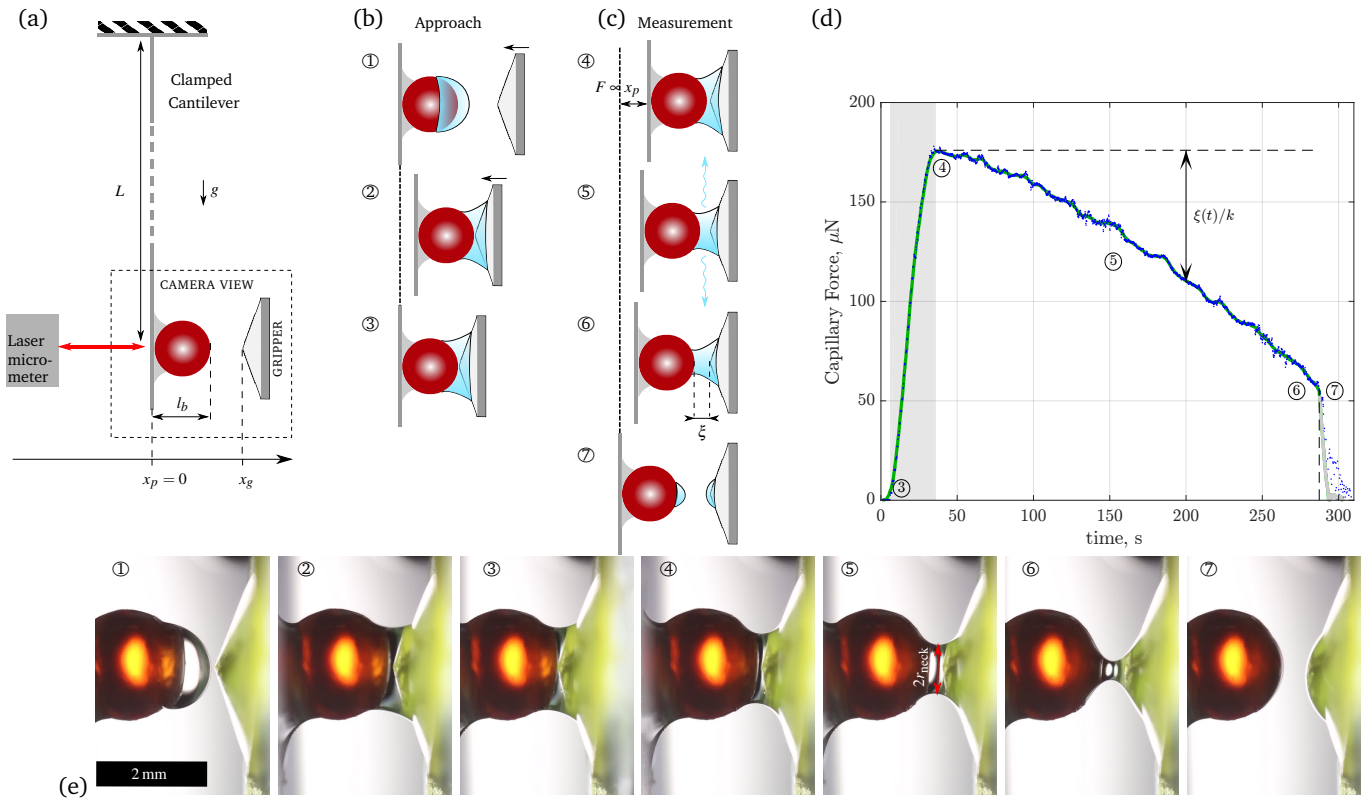

Fig. 2 Force measurement set-up and associated procedure. (a) Geometrical arrangement of the precision force measurement set-up. (b) Preparation of the set up. ① A droplet was deposited on the bead. ② The gripper was moved forward in the x-direction to form the capillary bridge. As the capillary bridge was created, the cantilever was deflected by the capillary forces. ③ The gripper was again moved forward until the cantilever was set back to its undeflected position. (c) Recording and drying of the capillary bridge ④ The experiment started by displacing the gripper backward. This motion deflected the cantilever by a distance x_p. ⑤ to ⑦ The capillary bridge dried and both the force F and the gap distance ξ were recorded until it broke-up. (d) Example of force and gap recording. The grey region corresponds to the end of the preparation to the measurement. The measurement was made in the blue region before the bridge broke-up between ⑥ and ⑦. (e) Images of the experiment illustrating configurations ① to ⑦.

imental set up comprised a clamped cantilever on which a glass sphere of 2 mm diameter was glued at a distance $L = 12.6$ cm from the clamping position. The width w and the thickness t of the cantilever were 1.27 cm and 100 μm respectively. The position of the cantilever x_p was initially zero. The deflection was measured with a non-contact displacement sensor (*Keyence LC2440*) with a resolution of about 0.2 μm. The gripper was mounted on a 3-axis motion system to easily set the gripper opposite to the sphere. The bridge axis was placed in the horizontal plane. The size of the bridge must also be significantly smaller than the capillary length in order to preserve the axisymmetry of the bridge. The whole procedure was imaged from the side with the same equipment as for the gripping experiment.

The experimental procedure is drawn in Figure 2b and c. A water droplet was deposited on the sphere ①. The gripper was moved towards the sphere until the liquid bridge formed ②, consequently the cantilever was deflected. The gripper was pushed forward in the same direction until the zero position of the cantilever $x_p = 0$ was reached ③. Here the sphere was in contact with the gripper. The attractive capillary forces generated by the liquid bridge were balanced by the repulsive normal contact force exerted by the sphere on the gripper. The gripper was displaced in the x-direction with steps of 20 μm from the zero position. The cantilever consequently deflected until the gripper stopped touching the sphere ④. The recordings started during stage ③ but data were processed from ④ only, Figure 2d.

We defined ξ as the gap distance between the tip of the gripper and the sphere. It was calculated as the difference between the motor position and the cantilever deflection. As the liquid bridge evaporated, its volume decreased which led to a reduced cantilever deflection ⑤. The rupture occurred abruptly when the configuration switched from ⑥ to ⑦.

The capillary force F was directly obtained through the deflection of the cantilever x_p when the gripper was not in contact with the sphere,

$$F = kx_p \quad \text{where} \quad k = \frac{3EI}{L^3} \tag{1}$$

was the stiffness of the cantilever, E the Young's modulus of the cantilever (steel) and $I = wt^3/12$ the second moment of area of the cross section. The spring constant has been directly measured using the classic pendant mass method. We obtained $k = 0.40 \pm 0.03\,\mathrm{N\,m^{-1}}$.

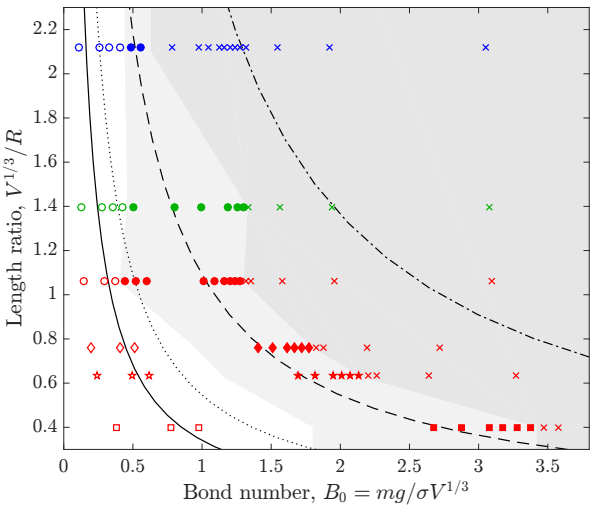

Fig. 3 Diagram of the gripper capability in terms of Bond number B_o and length ratio r. Three radii of curvature of the object were considered, $R = 625\,\mu$m (blue), $R = 950\,\mu$m (green), $R = 1250\,\mu$m (red). The symbols correspond to the liquid volume, $1.9\,\mu$L (○), $0.7\,\mu$L (◇), $0.4\,\mu$L (⋆) and $0.1\,\mu$L (□). Empty symbols and white background indicate the ability of the gripper to pick up the object but the impossibility to release it. Full symbols and light gray background indicate that the gripper can both pick up and release the object. Symbols × and dark gray background indicate that the gripper could not pick up the object. Solid, dotted, dashed and dot-dashed lines represents variations of volume, every other parameter being kept constant, with $\sigma = 72$ mN, $g = 9.81\,\mathrm{m\,s^{-2}}$, $m = 10$ mg and $R = 2$ mm (respectively $R = 1$ mm).

3 Results

3.1 Gripping performance

The ability of this gripper to pick and release millimeter-sized objects is first characterized. Relevant dimensional parameters are (i) the volume of water V used to pick up the object , (ii) the surface tension of water σ, (iii) the mass m of the object, (iv) the radius of curvature R of the spherical cap on top of the object, and (v) gravity g. An *educated guess*[24] would reveal that the density ρ of the liquid is not relevant, since the Laplace pressure induced by surface tension is much higher than the hydrostatic pressure inside this sub-millimeter liquid bridge. From these relevant parameters, we can build two dimensionless numbers, namely the Bond number and the length ratio:

$$B_o = \frac{mg}{\sigma V^{1/3}} \quad \text{and} \quad r = \frac{V^{1/3}}{R}. \tag{2}$$

The capability of the gripper as a function of (B_o, r) is summarized in the diagram of Figure 3. Three zones are identified: (i) the gripper can pick and release the object, (ii) the gripper can pick the object but not release it, and (iii) the gripper cannot pick the object. Variations of liquid volume for a given object (fixed mass m and curvature radius R) are represented as black lines in Figure 3. The object is initially bound to the gripper with a large volume (top left). If the starting point is in the white region the solid line describing variations of volume only will remain in this region meaning that the object will be picked-up but not released. At the opposite, if the picking starts in the dark grey region, the dot-dashed line describing the volume variation remains in this region meaning that it is impossible to pick-up the object. The dashed line starts in the light grey region meaning that it is possible to pick-up and release the object. As the volume is decreased (towards the bottom right), the line enters the dark grey region and the object is released. The dotted line transits between white and light grey regions meaning that depending on the starting volume it is possible or impossible to release the object. This inconsistent behaviour is likely due to contact angle hysteresis and triple line pinning that were not considered in this two-dimensional diagram.

The release performance of the evaporative gripper has also been quantified. The relation between the release time and the power used to warm up the liquid is represented in Fig. 4. For both the Joule effect and the laser heating, the release time τ is observed to be inversely proportional to the applied power P.

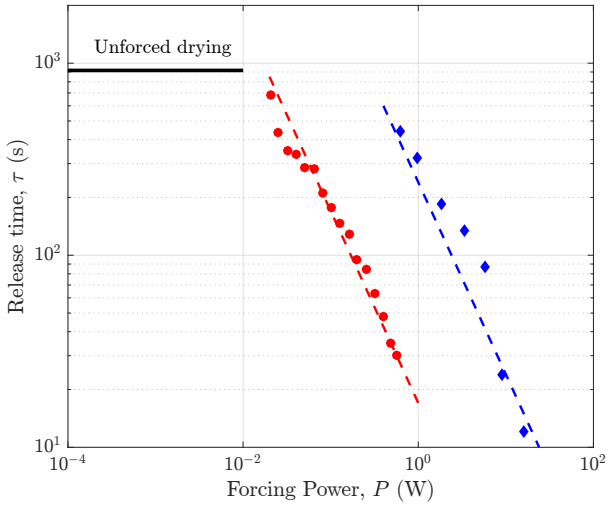

Fig. 4 Release time τ as a function of the input power P of the heating system (initial bridge volume $1.9\,\mu$L). (red) IR laser. (blue) Joule effect. Dotted lines correspond to equations 6 and 9, which confirm the scaling law $\tau \propto 1/P$. Unforced break-up time is reported as an asymptote (black line) in the log-log representation.

3.2 Gripping force

The gripping force F has been measured for the smooth cone and the textured cone as a function of temperature T, volume V, gap distance ξ. The raw measurement of F as a function of V for the smooth cone is displayed in Figure 5a. The force increases with the volume of the liquid bridge.

The effect of temperature, volume and surface texture are reported in Figure 6. We note that for a given volume and temperature the surface texture (in blue for the smooth cone and green for the textured cone in Figure 6) increases the adhesion force generated by the gripper. We analysed these experimental data with ANOVA tests to tell if the effect of volume, temperature and surface texture variations on the force generated by the gripper are statistically relevant or not. Statistical tests were performed

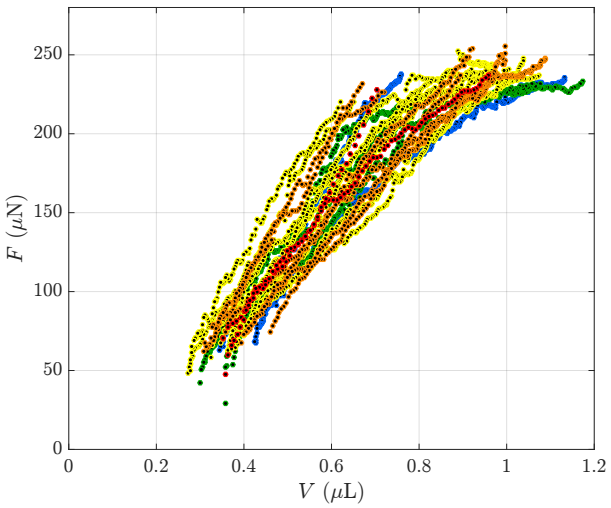

Fig. 5 Force generated by the smooth gripper as a function of the bridge volume. Colours indicate temperature (blue: T =23 °C; green: T =32 °C; yellow: T =42 °C; orange: T =47 °C; red: T =66 °C).

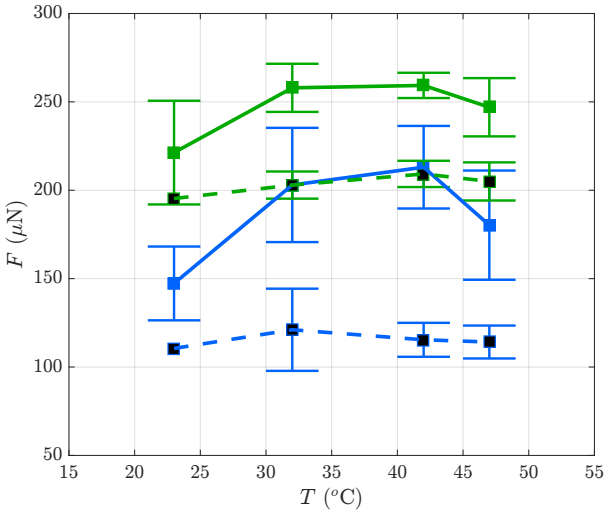

Fig. 6 Effect of temperature and surface texture on the gripping force. Coloured symbols and full line: barbule texture; Black symbols and dashed line: smooth cone; Blue (resp. green) corresponds to a volume of $0.4\,\mu$L (resp. $0.8\,\mu$L). Lines are guide for the eyes where only temperature varies. Error bars correspond to one standard deviation.

with quadratic models in volume and temperature,

$$F = a_0 + a_1 V + a_2 T + a_{11} V^2 + a_{12} VT + a_{22} T^2 \,, \qquad (3)$$

for both results obtained with smooth and textured grippers. Results are gathered in table 2. As expected the volume has a strong effect on the generated force for both grippers confirming the results in Figure 5a. However the surface texture has a non-trivial effect on the dependence of the force on the heating temperature. Temperature has no statistically relevant influence on the force in the case of the smooth cone (p-value >0.1) but it has one for the textured cone. In this case the force is maximal between 30 and 40 °C.

4 Models

4.1 Model of the release time

The experimental results of Fig. 4 on the evaporation time of the bridge can be rationalized with theoretical arguments. In the absence of convection, natural evaporation is only driven by the diffusion of water vapour, as initially modelled by Langmuir[25]. As a crude approximation, the liquid bridge is here replaced by a hemispherical droplet of the same volume. If the fine geometry of the bridge is taken into account it will only change the prefactor but not the scaling as long as the diffusion occurs across sections which area increases as the square of the distance to the droplet.

The diameter δ of this hemisphere is then $\delta(t) = (12V(t)/\pi)^{1/3}$. The relative humidity φ in the air surrounding the bridge is by definition the ratio of the partial vapour pressure P_v and the vapour pressure at saturation P_v^0. It satisfies the Laplace equation for pseudo-steady-state molecular diffusion in spherical coordinates, namely $\nabla^2\varphi = 0$. If we assume that gradients of φ are only radial, the vapour concentration profile is $\varphi(r) = \varphi_\infty + (1-\varphi_\infty)\delta(t)/2r$, where r is the radial coordinate and φ_∞ the relative humidity of the room during the experiment. The diffusive mass flux J is then calculated as $J = DM_w P_v^0 \nabla\varphi/(RT)$ which leads to $J = DM_w P_v^0(1-\varphi_\infty)\delta/(2r^2RT)$ where D is the diffusion coefficient of water vapour in air, M_w the molar mass of water, R the ideal gas constant and T the room temperature. Constants are gathered in table 3. A mass balance of water between liquid and gas phases then yields:

$$\rho \frac{dV}{dt} = -2\pi r^2 J \qquad (4)$$

The volume of the liquid bridge evolves from an initial value V_0 as

$$V(t) = V_0\left(1 - \frac{t}{\tau}\right)^{3/2} \text{ with } \tau = \frac{(3V_0/2\pi)^{2/3}\rho RT}{2DM_w P_v^0(1-\varphi_\infty)} \qquad (5)$$

Complete drying occurs at time τ, which varies as $V_0^{2/3}$. This time has been measured experimentally $\tau_{\text{exp}} = 917 \pm 44$ s and is reported in Fig. 4. The model evaluated with parameter values from Table 3 predicts $\tau = 2150$ s, which is larger than in experiments but still of the same order of magnitude. The discrepancy can be attributed to the replacement of the bridge geometry by a hemisphere, the assumption of a purely diffusive evaporation, and the fact that some liquid may remain at break-up.

When heat is brought to the bridge by laser or Joule effect, the evaporation is not driven by vapour diffusion anymore. For the heating strategy based on the Joule effect, the supplied power P yields an increase of thermal energy ηPt after time t, where the factor $\eta < 1$ is the fraction of produced heat that reaches the bridge. This thermal energy is used to first warm up the liquid to 100 °C (heat capacity c_p) and then to evaporate it (latent heat h). As the former requires about 7 times less energy than the latter, it can be neglected in first approximation. The energy balance then yields:

$$\eta Pt = h\rho\left[V_0 - V(t)\right], \qquad (6)$$

where $h = 2.26 \times 10^6$ J/(kg K) is the specific latent heat of water.

Table 2 ANOVA analysis dependence on volume V and temperature T with a quadratic model, Eq (3). (a) Smooth gripper, (b) Textured gripper. Significative p-values ($p< 0.05$) are marked in bold face. SS: Sum of Squares, DoF: Degrees of Freedom, MS: Mean Square, F: F-test,

(a)	SS ($\times 10^{-2}$)	DoF	MS ($\times 10^{-2}$)	F	p-value
Model, Eq 3	1.02	5	0.20	6.89	**<0.001**
V (a_1)	0.52	1	0.52	17.39	**<0.001**
T (a_2)	<0.01	1	<0.01	0.007	0.931
VT (a_12)	<0.01	1	<0.01	0.091	0.763
V^2 (a_{11})	0.02	1	0.02	0.681	0.413
T^2 (a_{22})	0.07	1	0.07	2.30	0.136
Residual	1.37	46	0.03		
Lack of Fit	0.03	6	<0.01	0.147	0.989
Pure Error	1.34	40	0.03		

(b)	SS ($\times 10^{-2}$)	DoF	MS ($\times 10^{-2}$)	F	p-value
Model, Eq 3	7.27	5	1.45	13.7	**< 0.001**
V (a_1)	0.75	1	0.75	7.09	**0.009**
T (a_2)	0.73	1	0.73	6.89	**0.010**
VT (a_12)	0.24	1	0.24	2.28	0.133
V^2 (a_{11})	0.05	1	0.05	0.446	0.505
T^2 (a_{22})	4.38	1	4.38	41.3	**<0.001**
Residual	13.35	126	0.11		
Lack of Fit	0.28	6	0.05	0.426	0.8604
Pure Error	13.07	120	0.11		

Table 3 Parameters and constants used in the models.

VARIABLES & COORDINATES			
V	Bridge volume	h_1	Bridge height
r, z	coordinates	ξ	Gap
t	time	F	Capillary force
R_s	Sphere radius	R_c	Cone contact radius
α	Cone opening angle	λ	Contact conformity
θ_1, θ_2	Contact angles	δ	Equivalent diameter
P_v	Water vapour pressure	φ	Relative humidity

EXPERIMENTAL PARAMETERS		VALUE
φ_∞	Ambient relative humidity	0.55
V_0	Initial bridge volume	0.5 to $2\,10^{-9}$ m^3 (μL)
T	Room temperature	293.15 K
P	Forcing power	0.1 to 10 W
m	Initial mass of liquid	0.5 to $2\,10^{-6}$ kg
η	Yield of evaporation process	-

CONSTANTS		VALUE
σ	Water surface tension	72 mN
P_v^0	Saturated water vapor pressure	$2.34\,10^3$ Pa
D	Diffusion coefficient of water vapor	$2.82\ 10^{-5}$ m^2.s^{-1}
M_w	Water molar mass	$18\,10^{-3}$ kg.mol^{-1}
R	Ideal gas constant	8.314 J.mol^{-1}.K^{-1}
ρ	Water density	$1.0\,10^3$ kg.m^{-3}
c_p	Water specific heat capacity	$4.2\,10^3$ J.kg^{-1}.K^{-1}
h	Water specific latent heat	$2.26\,10^6$ J.kg^{-1}
κ	Attenuation coefficient at 1455 nm	$2.6\,10^3$ m^{-1}

Therefore, the volume decreases linearly with time:

$$V(t) = V_0\left(1-\frac{t}{\tau}\right) \text{ where } \tau = \frac{\rho h V_0}{\eta P} \tag{7}$$

is the time of complete evaporation of the bridge. The yield η in equation (7) is estimated to 1.8% by fitting experimental data (Fig. 4).

When the bridge is evaporated by laser-induced heating, the amount of absorbed energy depends on the liquid thickness through the Beer-Lambert law. Therefore, the yield now depends on the thickness of the bridge, which scales as $\beta V^{1/3}$ where β is an unknown geometrical coefficient. For thin films, the absorbance is $\alpha\beta V^{1/3}$ where α is the attenuation coefficient of the electromagnetic wave sent by the laser (here 1455 nm) in water. The energy balance then yields

$$\left(\eta\kappa\beta V^{1/3}\right)P = -\rho h\frac{\mathrm{d}V}{\mathrm{d}t}. \tag{8}$$

The temporal evolution of liquid volume is then,

$$V(t) = V_0\left(1-\frac{t}{\tau}\right)^{3/2} \quad \text{where now} \quad \tau = \frac{3\rho h V_0^{2/3}}{2\eta\kappa\beta P} \tag{9}$$

Again, a comparison of this theoretical prediction to experimental data in Fig. 4 indicates that the factor $\eta\beta$ is about 11.8% (6 times more efficient than Joule effect).

Both models of forced evaporation suggest that the release time is inversely proportional to the input power P. However, its dependence to the initial liquid volume V_0 differs: it is proportional in the case of the Joule-induced evaporation, and less than proportional in the case of laser-induced evaporation. We expect that the use of a larger forcing power might keep reducing the releasing time, especially for the laser method that is not limited by thermal conduction in the gripper. For instance, we obtained a release time of $\simeq 10$ s with 0.5 W with the IR laser, we thus expect that using a more powerful laser of 50 W we would achieve the release in $\simeq 0.1$ s which would be close to industrial standards. The miniaturization of the components would also go with a reduction of the initial liquid bridge, and therefore with a substantial decrease of the evaporation time.

We showed that heating the bridge enhances the evaporation process and decreases the time needed to release the micro-object. However heating the bridge does not change the gripping ability, especially to release micro-objects. The ability to pick and release an object mainly depends on the geometry of the gripper.

4.2 Gripping force

The capillary force results from both the Laplace pressure and the tension at the contact line. In the absence of other effects, it is given by

$$F = 2\pi\sigma r_{\text{neck}} - \pi\sigma r_{\text{neck}}^2\left(\mathscr{C} + \frac{1}{r_{\text{neck}}}\right) \tag{10}$$

where r_{neck} is the neck radius, see Figure 2e, and $\mathscr{C}$ is the curvature at the neck along the z direction. Experimentally, $-\mathscr{C} r_{\text{neck}} \simeq 0.6-1.2$. In those condition the capillary force simply reads,

$$F = K\sigma r_{\text{neck}}\,. \tag{11}$$

where $K = 1-\mathscr{C} r_{\text{neck}} \simeq 1.6-2.2$. The experimental data are fitted by the above relation with $K = 1.5$, see Figure 8a, which is close to the range $[1.6, 2.2]$.

We now relate r_{neck} to the controllable parameters of the experiment, namely the volume V and the gap ξ. The exact relation between these parameters may be deduced by solving numeri-

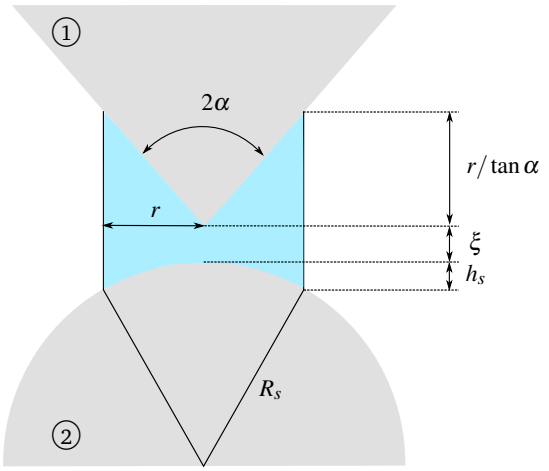

Fig. 7 Notations used to compute the equivalent radius of a volume of liquid between a cone and a sphere. $h_s = R_s(1-\sqrt{1-(r/R_s)^2})$

cally the Young Laplace differential equation in an axisymmetric frame. We here look for an empirical approximation to this relation. Conveniently, we define the equivalent radius r of a straight cylinder of same volume placed between the cone and the sphere with a gap ξ with the notations defined in Figure 7. The equivalent radius is given by

$$\frac{V}{\pi} = r^2\left(\xi + R_s\left(1-\sqrt{1-(r/R_s)^2}\right) + r\cot\alpha\right) - \frac{r^3}{3}\cot\alpha - R_s^3\left(1-\sqrt{1-(r/R_s)^2}\right)^2 + \frac{R_s^3}{3}\left(1-\sqrt{1-(r/R_s)^2}\right)^3. \quad (12)$$

The experimental data of the equivalent radius r, computed from Equation (12), are plotted in Figure 8b as a function of the neck radius. The experimental points collapse on a master line which can be approximated by an affine law as

$$\frac{r}{R_s} = 0.15 + \frac{r_{\text{neck}}}{R_s} \quad (13)$$

This empirical relation depends in a non trivial manner on the contact angles and on the pinning of the contact line. Indeed, we expect that small contact angles create a more curved bridge with a smaller neck radius r_{neck} than large contact angles would create. With the equations (11) and (13), we deduce the relation between the force and the equivalent radius of the bridge,

$$F = K\pi\sigma\,(r - 0.15R_s) \quad (14)$$

5 Discussion

The *contact conformity*[26] refers to the shape of the contact, as defined in solid mechanics. There is conformal contact when two solids fit one another similarly to a ball in spherical cup of identical diameter. For a capillary gripper, a contact is said conformal when it maximizes the capillary force, which is somehow related to the geometrical conformity borrowed from contact mechanics

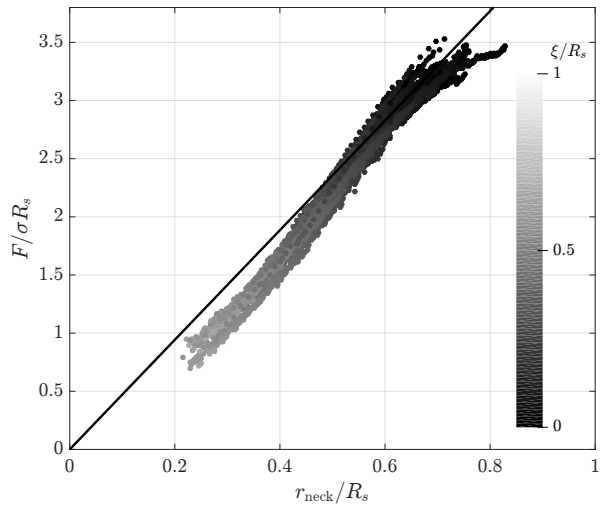

a.

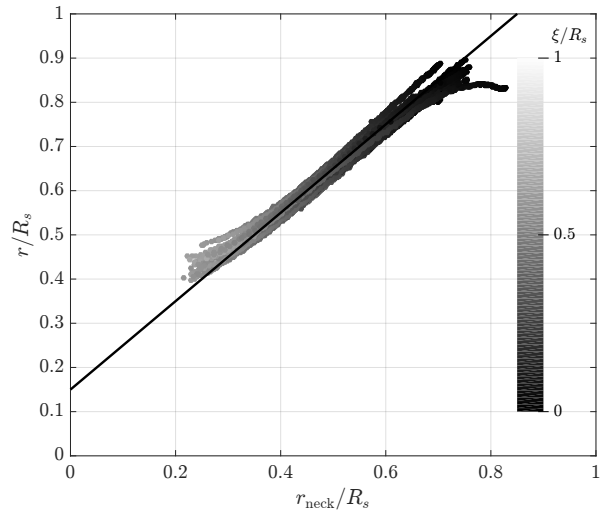

b.

Fig. 8 a. Normalized force of the gripper $F/\sigma R_s$ as a function of the neck radius r_{neck}. The solid line corresponds to the fit of the experimental data with F=$K\pi\sigma r_{\text{neck}}$ and $K = 1.5$. b. Normalized equivalent cylinder radius r/R_s computed from Equation (12). The black line correspond to the fit with Equation (13). The grey scale indicates the gap value ξ/R_s.

but not only[5]. The capillary force is maximized when two solids have a large contact area and a large curvature where the Laplace pressure jump occurs. One knows by intuition that the capillary force between a sharp cone and a sphere (small conformity) is lower than the one between a widely open cone and a sphere (large conformity). This may however be shown directly using the capillary force model derived hereinabove. If we take into account the full force, Equation (11), along with the equivalent radius, Equation (13), and its definition related to gap and volume, Equation (12), we observe that the force increases as the cone widens up then get reversed (*i.e.* $\alpha > 90°$). An example of the force as a function of the cone aperture angle α is plotted in Figure 9 using the following set of parameters: $V = 0.5\,\mu$L, $\sigma = 72$ mN, $\xi = 0.3$ mm and $R_s = 1$ mm.

To generalize the discussion to any capillary contact, we consider two solids of radii of curvature R_1 and R_2 respectively at the

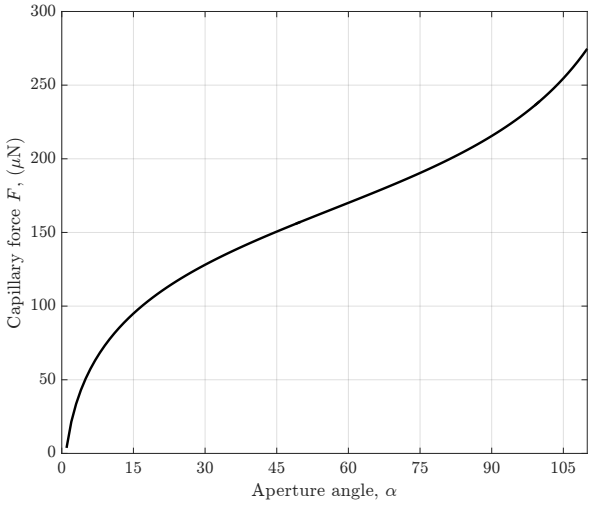

Fig. 9 Force of the gripper as a function of the aperture angle α. α >90° corresponds to reversed cone. This figure was plotted from Equations (11) and (12) using V =0.5 μL, σ =72 mN, ξ =0.3 mm and R_s =1 mm.

contact location. We also assume that the liquid makes a contact angle θ_1 on the first solid and a contact angle θ_2 on the second one. The capillary force F between two rounded solids reads[27],

$$F = 2\pi\sigma \left| \frac{R_1 R_2}{R_1 + R_2} \right| (\cos\theta_1 + \cos\theta_2) \tag{15}$$

At this step, we define the contact conformity as

$$\lambda = \frac{R_1 R_2}{\min(|R1|, |R2|)(R_1 + R_2)} \tag{16}$$

When the contact conformity is perfect, *i.e.* when two objects fit perfectly $R_1 = -R_2$, the conformity is infinite. Such configuration would maximize the attractive capillary forces. Conversely, if the first object has a much smaller radius of curvature than the second one, $|R_1| \ll |R_2|$ for instance, the conformity is $\lambda \simeq 1$ which leads to a capillary force proportional to the small radius of curvature R_1.

The concept of contact conformity may now be used to understand how our gripper works. The object has a radius of curvature R_s. To grab it, we use a wet cone for which the typical radius of curvature r^* depends on the liquid volume: during the pick-up phase, the conformity should be maximized, which suggests to use a large liquid volume (i.e. $r^* \gg R_s$). The picking conformity is then only driven by the object radius $\lambda \simeq R_s$. When the bridge dries, $r*$ decreases and so does λ. In some cases this might be sufficient to detach the object. However we noticed during preliminary tests that the object usually sticks on the side of a smooth cone, where the corresponding curvature is finite. On the textured gripper, barbules finally come into contact with the object as the liquid dries up. If the barbule radius R_b (radius of the cone at the contact position) is smaller than the one of the object $R_b \ll R_s$, the conformity is strongly reduced, which leads to a force of the order of the barbule radius R_b. With the textured gripper, the conformity at picking ($\lambda \sim R_s$) is much larger than conformity at releasing ($\lambda \sim R_b$), making detachment possible. Consequently, the object may detach from the gripper as soon as the decrease of conformity leads to a capillary force smaller that the object weight.

This capillary gripper releases objects without applying additional loads. We can therefore imagine using this technique on brittle objects in a pick-and-place context. In the case of the Joule effect stimulation, the thermal diffusion that occurs through the gripper would fix a lower limit to the release time even if the power is increased. The release time would be rather long compared to industry standards. However, we expect the release time to be strongly reduced, down to a fraction of second, if the IR-laser power is increased.

Even if millimeter-sized objects were considered as a first step, the precision of the stereolithography printing technique, *i.e.* 200 nm, allows to consider smaller objects. The barbules that we added to the gripper were also a first attempt and their shape can certainly be optimized. Any other shape giving a small conformity to the contact (*i.e.* having a large radius of curvature, such as spines or hairs) may be efficient. Some spine-like textured surfaces, inspired from cicada wings, have already been shown to be anti-mist and anti-biofouling[28] and might be of inspiration for the design of future grippers. Further optimization of the conformity at both the gripper and the texture scale would be interesting. For instance, a gripper with a radius curvature matching that of the picked object and textures with a very small radius of curvature compared to the object size might make a very efficient gripper.

An example of a conformal gripper producing a large initial capillary force is displayed in Figure 10a. This gripper fits the picked object when the liquid volume is large but as the liquid dries, the volume is reduced up to obtain several non conformal contacts, Figure 10b and c. At this step the capillary force is strongly reduced and the picked object should be released. However, in some cases, the object may remain attached to the gripper even after drying. This unwanted sticking would be due to some small capillary bridges of the order of the Kelvin radius (about 5 nm at 20 °C with 90% relative humidity) that would remain between the gripper and the object, Figure 10d. Those bridges have already been shown to create significant capillary forces[29]. Moreover they arise at a scale where Van-der-Waals forces also play a role in the adhesion between the object and the gripper.

The wettability of the gripper has not been varied in this study but is known to play an important role in the gripping of micro-objects. The IR-heating has also not been completely studied. It has recently been shown that the hot-spot location has an effect on the evaporation rate[30] which may be optimised to reduce the release time. The size of the smallest object that our gripper could seize and release may be estimated with the vertical asymptote of Figure 3, with a bond number of $B_0 \simeq 0.5$. If we consider a metallic object of density ρ =7000 kg m^{-3}bound with a volume V =0.1 μL of water σ =72 mN m^{-1}, the minimal dimension is L ~620 μm. Now, if the gripper and barbules shape are optimized and that inertial loads are used, one would expect to release much smaller objects.

In summary, we designed a 3D-printed capillary gripper based on a change of conformity of the contact for pick-up and release.

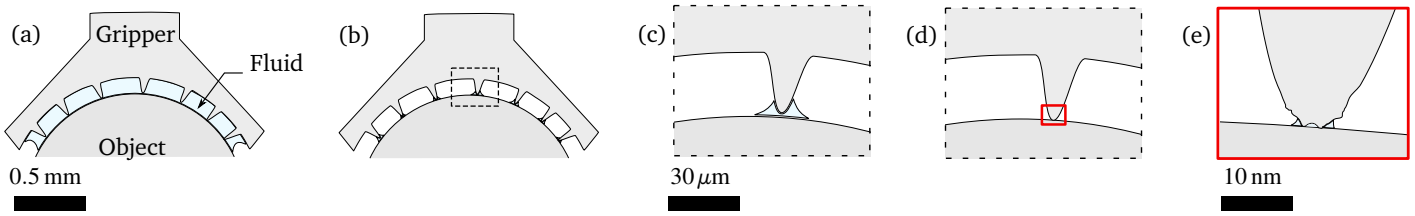

Fig. 10 Change of contact conformity during the drying process. (a) and (b) As the bridge dries, the contact is changed from one conformal macro-contact to several non-conformal micro-contacts. (c) close-up of a no conformal contact. The object is released when its weight is larger than the sum of the capillary forces of each bridge. (d) The release of the object may be limited by condensation of liquid at the scale of the kelvin radius ($\sim$5 nm).

The contact conformity is changed by evaporation of the liquid bridge. It switches scale, from the large cone to the small barbules. The evaporation may be forced by Joule effect or laser absorption to reduce the release time. The capillary force generated by the gripper depends directly on the contact conformity, *i.e.* the fitting between the gripper and the object. We use the capillary conformity as an efficient proxy to explain the pick and release mechanism. We hope that future capillary grippers will be designed using the contact conformity concept.

Conflicts of interest

There are no conflicts to declare.

Acknowledgements

Authors warmly thank F.N. Piñan Basualdo for letting them use his laser set-up. Authors thank FNRS financial support through research project T.0050.16 (Bioinspired passive liquid dispensing), FRIA grant, CHAR. RECH.-1.B423.18 (Tadrist L.) and FNRS GEQ 3D microstructuration and microengineering of surfaces with 3 photon lithography (2014-2016) (Nanoscribe GT Photonics, co-funding ULB/FNRS Grant UG01415F).

Notes and references

1 G. Fantoni, M. Santochi, G. Dini, K. Tracht, B. Scholz-Reiter, J. Fleischer, T. K. Lien, G. Seliger, G. Reinhart, J. Franke *et al.*, *CIRP Annals*, 2014, **63**, 679–701.

2 H. Jia, E. Mailand, J. Zhou, Z. Huang, G. Dietler, J. M. Kolinski, X. Wang and M. S. Sakar, *Small*, 2019, **15**, 1803870.

3 D. G. Grier, *nature*, 2003, **424**, 810.

4 P. Lambert, *Surface tension in microsystems*, Springer, 2013.

5 P. Lambert, *Capillary forces in microassembly: modeling, simulation, experiments, and case study*, Springer Science & Business Media, 2007.

6 C. Bark, T. Binnenbose, G. Vogele, T. Weisener and M. Widmann, Proceedings MEMS 98. IEEE. Eleventh Annual International Workshop on Micro Electro Mechanical Systems. An Investigation of Micro Structures, Sensors, Actuators, Machines and Systems (Cat. No. 98CH36176, 1998, pp. 301–305.

7 H. Grutzeck and L. Kiesewetter, *Microsystem Technologies*, 2002, **8**, 27–31.

8 P. Lambert, F. Seigneur, S. Koelemeijer and J. Jacot, *Journal of Micromechanics and Microengineering*, 2006, **16**, 1267.

9 M. Decre and R. Wolf, *Manipulation of objects with fluid droplets*, 2006, US Patent App. 10/539,968.

10 A. Vasudev, A. Jagtiani, L. Du and J. Zhe, *Journal of Micromechanics and Microengineering*, 2009, **19**, 075005.

11 A. Vasudev and J. Zhe, *Applied Physics Letters*, 2008, **93**, 103503.

12 S. Uran, R. Šafarič and B. Bratina, *Micromachines*, 2017, **8**, 182.

13 M. Saitou and T. Mizuno, *Method and apparatus for mounting electronic part*, 2008, US Patent App. 11/907,262.

14 Q. Zhang, H. Wang, Y. Gan, W. Huang and H. Aoyama, *Journal of Micromechanics and Microengineering*, 2017, **27**, 045006.

15 G. Fantoni, H. N. Hansen and M. Santochi, *CIRP Annals*, 2013, **62**, 17–20.

16 M. Cavaiani, S. Dehaeck, Y. Vitry and P. Lambert, 2018 International Conference on Manipulation, Automation and Robotics at Small Scales (MARSS), 2018, pp. 1–6.

17 M. Dafflon, *Préhenseurs, conditions et stratégies pour une micromanipulation de précision*, Epfl technical report, 2008.

18 Z. Fan, W. Rong, L. Wang and L. Sun, *Journal of Micromechanics and Microengineering*, 2015, **25**, 115011.

19 Z. Fan, L. Wang, W. Rong and L. Sun, *Applied Physics Letters*, 2015, **106**, 084105.

20 F. Apoorva, R. MacCurdy and H. Lipson, *System and methods for electrowetting based pick and place*, 2015, US Patent App. 14/415,414.

21 J. N. Israelachvili, *Intermolecular and surface forces, 3rd ed.*, Academic press, 2011.

22 F. Biganzoli, I. Fassi and C. Pagano, (ISATP 2005). The 6th IEEE International Symposium on Assembly and Task Planning: From Nano to Macro Assembly and Manufacturing, 2005., 2005, pp. 36–40.

23 F. Iovane, C. Pagano, L. Zanoni and I. Fassi, 1st CIRP-International Seminar on Assembly Systems, 2006, pp. 1–6.

24 C. J. Gommes and T. Gilet, *Chemical Engineering Progress*, 2018, **114**, 49–54.

25 I. Langmuir, *Physical review*, 1918, **12**, 368.

26 J. Skotheim and L. Mahadevan, *Physics of Fluids*, 2005, **17**, 092101.

27 P. Lambert, *Ph.D. thesis*, Capillary forces in micro-assembly, ULB, 2004.

28 T. Mouterde, G. Lehoucq, S. Xavier, A. Checco, C. T. Black, A. Rahman, T. Midavaine, C. Clanet and D. Quéré, *Nature materials*, 2017, **16**, 658.

29 A. Chau, S. Régnier, A. Delchambre and P. Lambert, *Journal of adhesion science and technology*, 2010, **24**, 2499–2510.
30 A. Askounis, Y. Kita, M. Kohno, Y. Takata, V. Koutsos and K. Sefiane, *Langmuir*, 2017, **33**, 5666–5674.